nature photonics

PROGRESS ARTICLE

PUBLISHED ONLINE: 28 MAY 2009 | DOI: 10.1038/NPHOTON.2009.89

# Infrared photovoltaics made by solution processing

Edward H. Sargent[1]

**Solution-processed photovoltaics offer a cost-effective path to harvesting the abundant resource that is solar energy. The organic and polymer semiconductors at the heart of these devices generally absorb only visible light; however, half of the Sun's power reaching the Earth's surface lies in the infrared. Flexible solar cells that harvest wavelengths beyond 1 μm were first reported in 2005. In three years they have increased over 10,000-fold in power conversion efficiency. The latest devices achieve power conversion efficiencies in the infrared of more than 4%, values comparable to those of their organic and polymer counterparts in the visible. Here we review the progress and prospects for the field, focusing on new insights into how quantum-dot solar cells operate and how these findings give guidance on optimizing these devices to their full performance potential.**

Photonic devices are most readily optimized for narrowband performance[1,2]. In solar energy conversion[3], however, the Sun's broad spectrum (Fig. 1a), spanning the visible, the near-infrared and a considerable portion of the short-wavelength infrared, means a broadband approach to photovoltaics is needed.

It is simplest to make a solar cell using a single semiconductor junction. Photons more energetic than the bandgap of the light-absorbing semiconductor are then absorbed and harvested, whereas those lying below the bandgap remain unabsorbed. Simple analysis of the Sun's power spectrum reaching the Earth implies an optimal choice of bandgap: decreasing the bandgap increases the fraction of the Sun's power absorbed, but comes at the cost of lowering the open-circuit voltage (see Table 1). For unconcentrated rays, the optimal bandgap of such a single-junction cell is 1.13 eV, corresponding to 1.1 μm in the short-wavelength infrared.

Multi-junction solar cells, wherein semiconductors with different bandgaps sequentially extract power from their respective portions of the Sun's broad spectrum, lead to higher overall solar power conversion efficiencies (Fig. 1b). A first large-bandgap cell absorbs higher-energy photons only, and provides a correspondingly large open-circuit voltage; the next cells absorb the lower-energy photons and provide additive contributions to the open-circuit voltage. The optimal bandgap choices for each member of the multi-junction stack are summarized in Fig. 1b. Both layers in the tandem (two-junction) cell are in the infrared, as are two of the three layers of the optimum three-junction photovoltaic stacked device. Use of a triple-junction architecture increases the upper bound on the power conversion efficiency for unconcentrated AM1.5 reference irradiance conditions (see Table 1) from 32% to 49%.

The benefits of matching a solar cell's response to the Sun's spectrum are widely used in commercially available photovoltaics. Silicon offers the optimal single-junction bandgap, although its low absorption from 600 nm out to its bandgap at 1,100 nm necessitates the use of thick absorbing layers and a considerable amount of crystalline silicon. Epitaxially grown triple-junction compound semiconductor devices have reached 41% AM1.5 power conversion efficiency with the aid of optical concentration[4].

The single-crystal solar cells that have led to these performance records have several practical disadvantages: high materials cost, high energy payback time and a lack of physical flexibility. As a result, large-area-compatible photovoltaics, such as those based on amorphous silicon, copper indium gallium selenide, cadmium telluride and photochemical dye-sensitized devices, have seen great advances and now offer impressive performance[5].

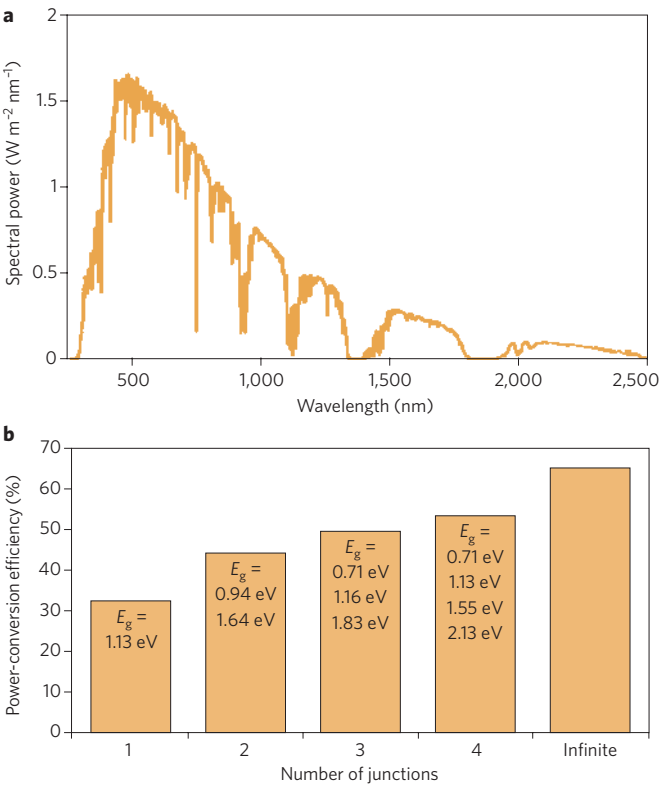


**Figure 1 | The Sun's power spectrum reaching the Earth and its consequences for solar cell design. a**, The unconcentrated AM1.5 solar spectrum. **b**, The maximum power conversion efficiency[54] that an *n*-junction ($n = 1, 2, 3, \infty$) solar cell can achieve for unconcentrated AM1.5 illumination. The optimal bandgap(s) for the corresponding junction(s) are indicated within the bars of the plot. For example, if only a single bandgap is used, the maximum PCE is 31.5%, and the bandgap is optimally chosen to be 1.13 eV.

Solution-processed materials, where the active light absorber is dispersed in a solvent that evaporates during the photovoltaic manufacturing process, offer particular promise with respect to cost per area. Being typically non-crystalline or polycrystalline, often with functional groups included for the passivation of surfaces, they present no issue of lattice-matching, nor the requirement for a rigid

[1]Department of Electrical and Computer Engineering, University of Toronto, 10 King's College Road, Toronto, Ontario M5S 3G4, Canada.
email: ted.sargent@utoronto.ca

**Table 1 | Important terms for photovoltaic performance.**

| | |
|---|---|
| PCE | Power conversion efficiency. The ratio of electrical power provided by the cell to the optical power incident on the device. |
| AM1.5 | Air Mass 1.5. A standard terrestrial solar spectral irradiance distribution. |
| Isc | Short-circuit current. The current that flows in a photovoltaic device when illuminated, and when its contacts are shorted. This value is generally greater than the actual current it can pass when a real load is powered by the cell. |
| EQE | External quantum efficiency. The ratio of the number of electrons flowing per second under short-circuit current conditions to the number of photons illuminating the device each second. |
| IQE | Internal quantum efficiency. Same as for EQE, except that it considers the number of photons absorbed by the device each second. |
| $V_{oc}$ | Open-circuit voltage. The voltage provided by an illuminated photovoltaic device when no external load is connected. |
| FF | Fill factor. The ratio of the actual power a solar cell can supply to the maximum predicted by the product of its short-circuit current and its open-circuit voltage. |

crystalline substrate. Large-area coverage can be achieved by low-temperature spray-coating or inkjet printing from the solution phase, often combined with roll-to-roll processing[6], leading to coating using continuous-flow methods instead of sequential wafer handling.

## Device architecture and performance

This review focuses on recent progress in solution-processed photovoltaics that provide infrared power conversion. This focus is motivated by the urgent need for low-cost solar cells with improved power conversion efficiencies, and the need to incorporate infrared absorption into any solar cell striving to achieve high power conversion efficiencies.

Figure 2 introduces the device architecture and materials processing strategy shared by recent solution-processed infrared photovoltaics[7–11]. The most efficient devices have been made by solution-processing of semiconductor colloidal quantum dots (CQDs) (Fig. 2a, b). These nanoparticles are spectrally tunable through the quantum size effect. They are synthesized in solution with the aid of a ligand such as oleic acid that controls growth, produces a stable colloid and passivates the nanoparticles' surfaces. The long passivating ligands must be replaced by shorter molecules to increase the mobility of charge carriers in thin-film devices. Schottky-contacted solar cells (Fig. 2c) use a transparent ohmic bottom contact followed by the light-absorbing nanocrystal layer and topped with a shallow-work-function metal electrode. A 4×4 array of such devices on a glass substrate of dimensions 2.5 × 2.5 cm is depicted in Fig. 2d.

Progress in solution-processed infrared photovoltaic performance is summarized in Fig. 3 and Table 2. Performance is quantified in terms of the monochromatic power conversion efficiency at specific wavelengths. Because high-efficiency solar cells will require multiple junctions, it is necessary to examine the individual performance of each of the junctions that will become combined in future multi-junction cells. Two infrared bandgaps are of particular interest, corresponding to the two optimal infrared choices in a three-junction multi-junction photovoltaic device: ~1 μm and ~1.5 μm. (Substantial research effort in recent years has extended organic solar cell absorption towards the red within the visible spectrum. An excellent summary is available elsewhere[12]. Herein I focus instead on devices that gather a large portion of the infrared.)

Figure 3 and Table 2 show that, since the first report in 2005, solution-processed infrared solar cells have rapidly progressed to useful efficiencies (>4% monochromatic power conversion efficiency). Near 1 μm wavelength, pure-organic and pure-quantum-dot approaches vie for the performance record; whereas near 1.5 μm, pure-quantum-dot approaches alone have so far provided record efficiencies.

## Device mechanisms of operation

The solar cells providing greater than 1% monochromatic power conversion efficiency near 1.5 μm have much in common[7,8,10,11]. Each used a pure quantum-dot active layer, rather than a bulk heterojunction formed by a polymer–nanocrystal mixture. Each relied on forming simple metal contacts — one deep in work function, one shallow — to this light-absorbing semiconductor quantum-dot layer. In the best-performing devices reported so far, no interlayers were required, such as those intended to block one type of carrier and extract another, as used in type-II heterojunction solar cells.

The mechanism of operation of this simple class of devices has recently been investigated in detail[10,13] and is depicted in the spatial band diagrams of Fig. 4c and d. The light-absorbing layer is a p-type semiconductor having a Fermi level that is closely aligned with the work function of the transparent contact. Little band-bending is expected at this junction, and holes can be readily extracted through the junction. In contrast, the p-type semiconductor and shallow-work-function metal contact, such as Al, Mg or Ca, differ by at least 0.6 eV in work function, producing band-bending near this interface. The resultant Schottky barrier[14] favours the extraction of electrons from the device while presenting a barrier to hole withdrawal.

From the perspective of charge-carrier transport, drift and diffusion play important roles in the operation of this device. Figure 4 depicts a drift-dominated device (a, b) and a diffusion-dominated device (e, f) to emphasize the key requirements on transport in these two cases. It also shows the spatial band diagram of a Schottky device in which drift and diffusion play quantitatively comparable roles (Fig. 4c, d). These balanced drift–diffusion devices are representative of the best infrared CQD photovoltaics.

In the light-absorbing semiconductor portion of the metal–intrinsic–metal device of Fig. 4a, the use of asymmetric contacts, one having a deep work function, the other shallow, produces a built-in field across the entirely depleted semiconductor. Under illumination,

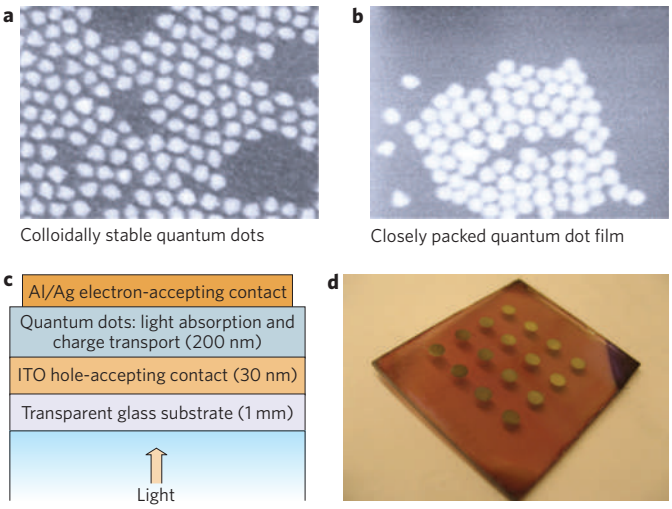


**Figure 2 | Architecture of a typical solution-processed infrared photovoltaic cell. a–c** Scanning electron micrographs of as-synthesized colloidal quantum dots (**a**) originally capped with long ligands that are processed in solution to provide short-ligand-capped (ligand-exchanged) nanoparticles (**b**). These are then cast to form a device. **c**, Schematic of a Schottky-barrier CQD device using a p-type semiconductor clad by an ohmic transparent bottom contact and a top contact with a shallow work function. ITO, indium tin oxide. **d**, Photograph of a 4×4 array of devices on a glass substrate, 2.5 × 2.5 cm in size.

this built-in field propels photogenerated electron–hole pairs in opposite directions.

For a device to have high internal quantum efficiency, carriers must be extracted before they recombine. This requires that the mobility $\mu$ of each carrier exceed $\tau V_{bi}/d^2$, where $V_{bi}$ is the built-in potential, $\tau$ is the carrier lifetime, and $d$ is the device thickness. The best recent demonstrations have shown $V_{bi}$ between 240 mV (ref. 10) and 400 mV (ref. 7) with depletion regions ranging from 100 to 150 nm. Radiative lifetimes in Pb-chalcogenide materials have been reported to be as long as 10 μs, with 1–5 μs more typical. Together, these parameters mandate the need for mobilities exceeding $1 \times 10^{-4}$ cm$^2$ V$^{-1}$ s$^{-1}$ to achieve efficient transport from the depletion region. Measurements of mobilities in films fabricated identically to those used to make CQD photovoltaic devices have so far yielded at best[9] $2 \times 10^{-3}$ cm$^2$ V$^{-1}$ s$^{-1}$, with $10^{-4}$ cm$^2$ V$^{-1}$ s$^{-1}$ more typical of the slower carrier, typically electrons[13]. Thus, although marginal, typical values are sufficient for efficient carrier extraction from the depletion region.

This high efficiency of electron–hole pair extraction from a 100-nm or thicker depletion zone in CQD devices contrasts with the field of polymer photovoltaics. In polymer metal–intrinsic–metal devices, external quantum efficiencies have been low, typically below 1% (ref. 15), compared with the 60% and above recently seen in CQD devices. Two factors explain this contrast. Electron–hole pairs exist as bound excitons in polymers owing to low permittivity of these materials; as a result, in the absence of very rapid charge separation, recombination occurs rapidly, typically on the nanosecond timescale. Although sufficiently high mobilities could overcome this, disordered polymer semiconductors typically show hopping with the lower mobility (electrons) at or below the $1 \times 10^{-4}$ cm$^2$ V$^{-1}$ s$^{-1}$ range.

Diffusion of minority carriers also has a important quantitative role in the best CQD photovoltaics. To illustrate this process, Fig. 4e and f shows a pn-junction device in which, as a result of high doping, the depletion region is thin, and most photocarriers are generated in a quasi-neutral region. In these regions, minority carriers are required to diffuse to the junction to have the benefit of transport into their majority carrier regions by means of the built-in field. The minority-carrier diffusion length for each carrier must exceed its quasi-neutral region thickness for diffusion to be an efficient transport process contributing to high quantum efficiency. In CQD devices, estimates of minority carrier diffusion length are typically in the 100-nm range[10,16]. As this is comparable to the depletion depth near the Schottky junction, carrier diffusion contributes appreciably to the extraction of photocarriers in devices such as illustrated in Fig. 4c and d. For comparison, organic photovoltaic devices are highly reliant on diffusion, in their case the diffusion of excitons having a 5–20-nm characteristic diffusion length[17]. In organics, it is this short exciton diffusion length that necessitates the use of bulk heterojunctions[18,19] or nanoporous architectures[20] to overcome the extraction–absorption compromise. Silicon photovoltaics also rely on long-length-scale diffusion of one carrier: although silicon's length scale of hundreds of micrometres for absorption is orders of magnitude greater than that of organics and CQD films, so too is its minority carrier diffusion length, a consequence of the long lifetime of electron–hole pairs in indirect-bandgap silicon, combined with their high mobility.

## Challenges and future prospects

**Overcoming the absorption–extraction compromise.** The best-performing solution-processed devices reported so far absorb only a fraction (10–70%, depending on wavelength) of incident photons with energies greater than the material's quantum-confined bandgap. The obvious solution is to thicken the active region; but it has been found that, although it increases absorbance, this reduces the efficiency with which charge carriers are extracted. We term this the absorption–extraction compromise.

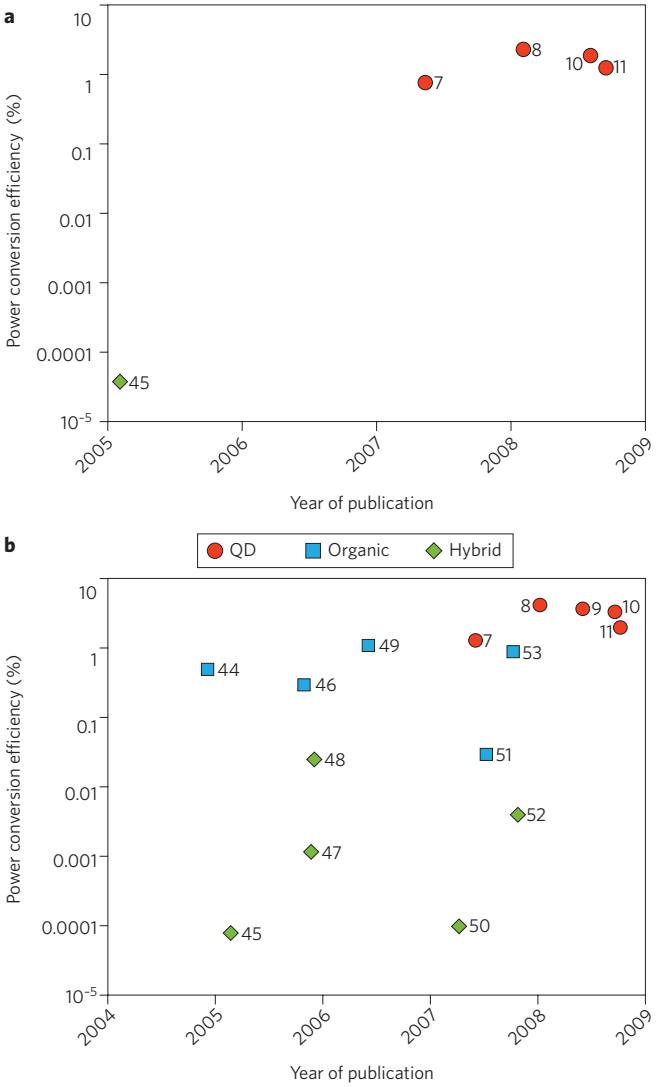


**Figure 3 | Progress in infrared monochromatic power conversion efficiency of solution-processed photovoltaics. a**, At 1.5 μm wavelength; **b**, at 1 μm wavelength. Organic refers to purely organic or polymer devices; QD refers to devices consisting purely of quantum dots (although they may be passivated or otherwise functionalized using short organic ligands); and hybrid refers to devices that combine an organic/polymer layer with an inorganic layer, or that use a mixture of polymer and quantum dots. Numbers are reference numbers; see also Table 2.

The depletion widths and diffusion lengths recently reported are surprisingly large, at around 100 nm, an order of magnitude greater than in organic semiconductors; and yet are still almost an order of magnitude less than the minimum absorption length for light just above the bandgap in CQD films. High external quantum efficiencies (EQEs) in the visible are therefore achieved, but high EQE is needed across the devices' entire absorbing spectrum. Near the bandgap, the absorbance $\alpha$ is of the order of $10^4$ cm$^{-1}$, demanding the equivalent of ~1 μm of planar material to achieve complete absorption. In such a thickness of CQD materials today, carriers will be lost to recombination due to existing transport limitations.

Within the planar architecture, the solution is to improve mobilities. Ideally carrier mobilities need to be at least two orders of magnitude greater than the typical $1 \times 10^{-4}$ cm$^2$ V$^{-1}$ s$^{-1}$ reported in CQD films. Figure 5 illustrates the degrees of freedom available to reach higher carrier mobilities.

**Table 2 | Infrared photovoltaic power conversion efficiencies near two key infrared photon energies.**

| Date | PCE at ~1.5 μm | PCE at ~1 μm | Type | Reference |
|---|---|---|---|---|
| Nov 2004 | | 0.5% | Org | 44 |
| Jan 2005 | 0.00004% | 0.00008% | Hyb | 45 |
| Oct 2005 | | 0.3% | Org | 46 |
| Nov 2005 | | 0.001% | Hyb | 47 |
| Nov 2005 | | 0.025% | Hyb | 48 |
| Apr 2006 | | 1.1% | Org | 49 |
| Mar 2007 | | 0.0001% | Hyb | 50 |
| Apr 2007 | 0.8% | 1.3% | QD | 7 |
| Jul 2007 | | 0.03% | Org | 51 |
| Sept 2007 | | 0.004% | Hyb | 52 |
| Oct 2007 | | 0.9% | Org | 53 |
| Jan 2008 | 2.4% | 4.2% | QD | 8 |
| Jan 2008 | | 3.7% | QD | 9 |
| Jul 2008 | 1.7% | 2.3% | QD | 10 |
| Sept 2008 | 1.3% | 2% | QD | 11 |

QD, quantum dot; Org, organic, including small molecule, polymer and $C_{60}$ mixtures; Hyb, a hybrid mixture of quantum dots with organic/polymer. In many cases the monochromatic power conversion efficiency at the wavelength of interest was not reported explicitly in the cited work; however, external quantum efficiency (often in the form of a spectrum), open-circuit voltage and fill factor were provided, and thus PCE was estimated as PCE = EQE × ($qV_{oc}/E_{photon}$) × FF (see Table 1), where $q$ is the charge of an electron. The highest EQE in the range 950–1,000 nm was used for each reference. In general, EQE, $V_{oc}$ and FF can vary with illumination intensity, yet the measurements in the table were not taken at a single standard illumination intensity.

The spatial separation of the quantum dots, $w_b$, determines the width of the energetic barrier that carriers must penetrate to reach an adjacent dot. The primary strategy to reduce this has been the replacement of long ligands, used in synthesis, with shorter ligands[21]; recent evidence shows that chemical treatments that improve interpenetration between the ligand shells surrounding the dots offers similar transport benefits. Reducing the inter-dot barrier height, $h_b$, has been achieved[22] by using bidentate ligands, sometimes termed linkers, in which the bridging group, such as benzene, provides for delocalization of electrons or holes[23].

Mobilities in the range $10^{-1}$ to 1 $cm^2\ V^{-1}\ s^{-1}$ have been reported in CQD solids made into field-effect transistor (FET) structures[24]. Here, delocalization of charge carriers among quantum dots was achieved through the formation of an ordered lattice of nanocrystals — a superlattice. Referring to Fig. 5, $w_d$ and $w_b$ were made highly periodic through monodispersity and ordering, increasing the penetration of electron and hole wavefunctions into adjacent dots. Translating these high mobilities into materials that can be combined to form photovoltaic-relevant device architectures remains a challenge for CQD photovoltaics. It seems likely that there exists no fundamental incompatibility between the nanoparticle ordering and ligand chemistries that lead to high mobilities in CQD films; but these demand careful control over film morphology to avoid a low shunt impedance resulting from cracks and pinholes. The influence of mobility-enhancing surface treatments on net doping must be taken into account, and may necessitate changes in device architecture, such as a move to pn-junction devices. In materials possessing high densities of traps, the extent to which these traps are filled determines the effective mobility observed. In FET measurements, the application of a gate bias typically fills many of the deeper traps, with channel modulation revealing the mobility of the shallower traps or the subbands. In contrast, a photovoltaic device's quasi-Fermi levels are determined by the competition between optical generation on one side, and extraction and recombination on the other. This competition generally leads to carriers of at least one type having a quasi-Fermi level considerably removed from their band-edge, thus leaving traps of considerable depth exposed. Traps may in this case dominate mobility under realistic operating conditions.

A strategy complementary to transport enhancement is to break the extraction–absorption compromise. This is achieved by forming a three-dimensional structure in which photogenerated excitations are always close to a charge-separating junction. In contrast with the simple planar Schottky architecture, the active region is structured on the length scale of carrier transport, as in bulk heterojunction (Fig. 6a) and nanoporous (Fig. 6b) architectures.

In the latter case, a porous transparent electrode or electron-acceptor is infiltrated with a light-absorbing material. The device can be made thick, and prospectively fully optically absorbing, while nevertheless ensuring that electron–hole pairs lie within an extraction length (based on drift, diffusion or both) of a charge-separating junction. This approach was recently investigated and found to lead to infrared photovoltaic devices[11] having 2% monochromatic power conversion efficiency in the infrared. Thus, these first attempts have so far led to efficiencies comparable, but not yet superior, to simple planar devices. New mechanistic insights obtained in planar photovoltaic devices now indicate that an improved choice of electrode — such as $TiO_2$ to form a type-II heterojunction or a shallow-work-function transparent oxide such as n-ZnO to form a Schottky barrier — would offer greater advantages when working with p-type infrared-absorbing CQD semiconductors.

**Engineering nanoparticle passivation.** Another potential compromise looms in devices made from a collection of colloidal quantum dots. On the one hand, close spacing among nanoparticles is desired for efficient charge carrier transport through the material; on the other, nanoparticles' surfaces are generally thought to require excellent passivation to maximize charge carrier lifetimes, and the molecules used in passivation tend to be bulky and thus stand in the way of dense packing.

Recent studies have clarified the means, and the role, of passivation, and have suggested that very short (significantly less than nanometre-sized) passivating ligands can help[25]. These findings have arisen in the context of an investigation into the precise role of thiol-terminated ligands and crosslinkers in infrared CQD photovoltaic performance. Thiols have been seen to improve performance in a wide range of reports; the principal reason for this was given as improvements in mobility when short thiol-terminated ligands replaced longer original[7,10,16,26,27] ligands. It was realized that such transport enhancements could not, on their own, account for even the majority of the improvement thiols produced[25]. Further investigations showed a marked enhancement in photoluminescence quantum yield of CQD films upon thiol exposure, suggesting a role for improved passivation, especially of deep traps that serve

as recombination centres. (In the picture of Fig. 5, the passivation of deep traps implies that the distribution of trap depths $h_t$ was clustered close to the bands, rather than near the midgap. Midgap traps capture electrons and holes with similar probability, leading to recombination instead of lifetime extension.)These observations suggested a picture of excited photocarriers familiar in organic photovoltaics[28]: excitons can either recombine or dissociate, where the latter outcome produces longer-lived states available for efficient extraction. It has been proposed that shallow traps for carriers of one type can produce such 'way stations' along the route to efficient, separate carrier extraction. These findings resonate with recent discoveries of the role of thiol treatments in photoconductive photodetectors in which thiol-treated samples retained only the short-lived traps associated with comparatively rapid temporal response[29]. Chemically, this is attributed to the reduction in thiols of species such as $PbSO_4$ associated with deep trapping.

**Contacts.** The metal–semiconductor junction in Schottky barrier devices has the crucial role of establishing a built-in potential, and a field to separate electron–hole pairs. In light of the sub-optimal open-circuit voltages and fill factors seen in devices so far, this junction requires, and has room to benefit from, considerable further optimization.

The first report of a Schottky junction between CQD film and a metal[14] yielded an appreciable built-in potential, but one still noticeably lower than the work function difference between the metal and the p-type semiconductor. This led to the suggestion of Fermi level pinning occurring at the semiconductor–metal interface. Such effects are important in photovoltaics as they limit the open-circuit voltage that a device can provide.

Fermi level pinning at midgap can be explained in terms of deep traps either inherent in the semiconductor or arising because of changes to the semiconductor (such as introduced by sputtering damage during metal deposition) near its surface. Further evidence of this effect was recently provided[10], in which the amplitude and polarity of the open-circuit voltage depended not only on the inherent work function difference between the two contacts, but was influenced by materials processing: the choice of which contact resided on the substrate, and which contact was sputtered atop the film at the end of film processing, influenced the polarity and amplitude of photovoltaic open-circuit voltage. Such effects were explained by invoking the effect of contact deposition technique on surface states and interface layers.

Schottky barrier photovoltaics are in general limited to providing open-circuit voltages of order half of the bandgap[3]. In smaller-bandgap (infrared) devices, this limitation may not substantially lower the open-circuit voltage compared with the idealized pn-junction. In general, however, especially for higher bandgaps, both pn-junction and heterojunction photovoltaics offer the potential of higher open-circuit voltages than in Schottky devices. Realization of a pn-junction device is thus desirable, and should be achievable in view of the ambipolar nature of PbS and PbSe (ref. 24); however, the need for highly reducing treatments, carried out in the solid state, such as those involving hydrazine, suggests that new processes must be developed that can create a controlled junction rather than converting the entire film. Heterojunction devices based on colloidal quantum dots are starting to be explored[30,31] and hold great promise.

**Multi-exciton generation.** Multi-exciton generation (MEG), also known as carrier multiplication, refers to the creation of two or more electron–hole pairs by a single, energetic absorbed photon[32]. Its potential advantages in solar energy conversion reside in making more efficient use of photons whose energies are well in excess of the light-absorbing semiconductor's bandgap. Initially, the absorption of such photons results in electron–hole pairs having considerably greater energy than bandgap excitons. In the absence of carrier multiplication, the electron and hole rapidly relax, through thermal intraband dissipation of energy, to the

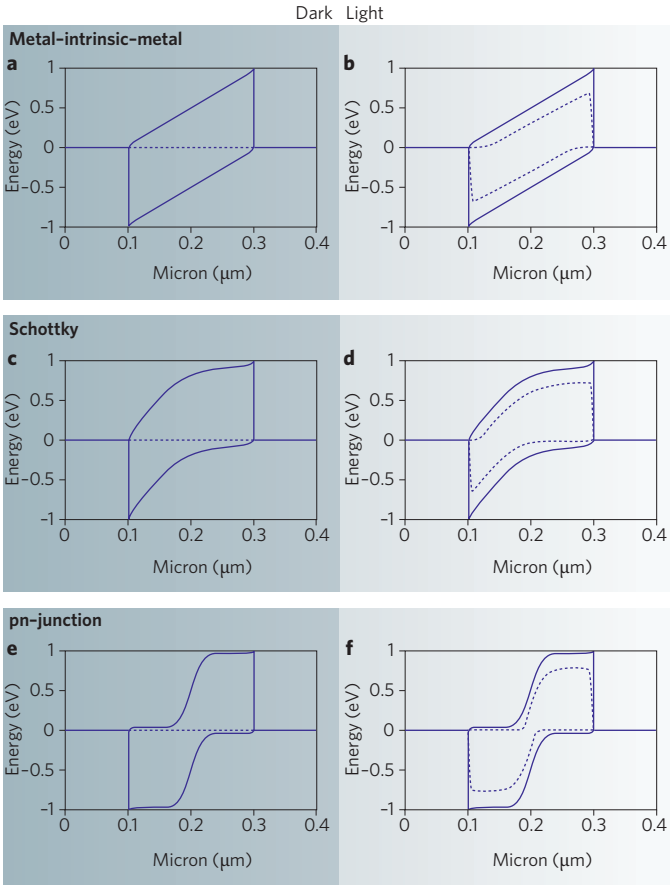


**Figure 4 | Drift and diffusion of charge carriers in photovoltaics.** The figure provides spatial band diagrams in the dark (left) and under solar illumination (100 mW $cm^{-2}$, right) for a metal–intrinsic–metal, metal–p-type–metal (Schottky), and pn-junction solar cell. The metal–intrinsic–metal device (**a**,**b**) shows uniform band-bending throughout its extent, produced by the work function difference between its electrical contacts. Electrons and holes are separated and extracted by the action of the resultant field. The Schottky device (**c**,**d**) involves one Schottky contact (produced by a large work-function difference between the shallow work-function metal on the left and the p-type semiconductor) and one substantially ohmic contact on the right. A depletion region forms, but the depletion depth is limited by the doping (in this case $1 \times 10^{17}$ $cm^{-3}$) of the semiconductor. In the undepleted quasi-neutral region on the right half of the device, minority electrons generated by photoexcitation are required to diffuse to the edge of the depletion region, where the field sweeps them out. The pn-junction device (**e**,**f**) also forms a depletion region, narrow for the doping levels chosen herein, such that most photocarriers are required first to diffuse in order to reach the charge-separating junction.

bandgap. As a result, they lose the energy they held in excess of the bandgap. This underuse of the Sun's energetic photons accounts for the 31.5% single-junction solar energy conversion limit of Fig. 1. In contrast, in MEG an energetic electron–hole pair well above the bandgap may, for example, produce a pair of bandgap-energy excitons. Although the resultant energy of each exciton is the same as in the preceding case, the number of particles is doubled: if efficiently extracted, these excitons offer an increased short-circuit current density.

In view of the Sun's spectral distribution across the visible and infrared, if MEG is to provide enhanced solar power conversion it will require a small-bandgap light-absorber[33]. Its practical application is therefore of greatest potential interest in infrared CQD solar

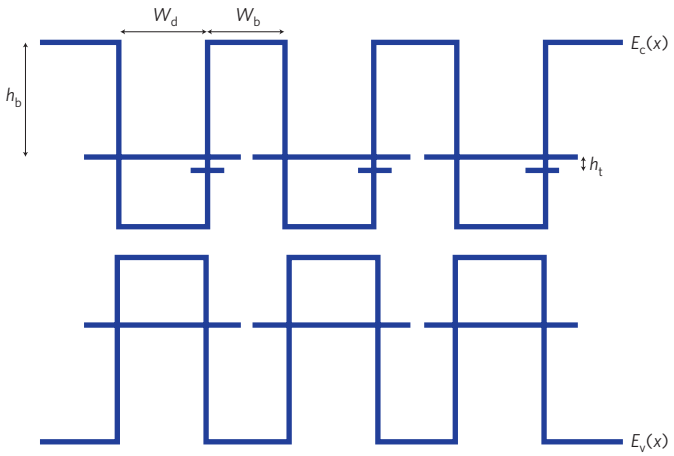


**Figure 5 | Spatial band diagram of a colloidal quantum-dot solid.** The diameter of the quantum dot is depicted by $w_d$, the spacing between dots by the barrier width $w_b$, the height of the barrier measured relative to the first quantum-confined state by $h_b$, and the energy depth of traps relative to the first quantum-confined state by $h_t$. $E_c$ and $E_v$ refer to the conduction and valence band edges, respectively, of the constituent materials. Monodispersity of quantum dots leading to a consistent $w_d$ produces energetic alignment of confined states within the solid. A thin, consistent barrier width and height also favour carrier delocalization and transport. Passivating deep traps leaving either no traps, or only shallow traps ($h_t$ < 0.1 eV), also favours efficient transport within a band.

cells. Colloidal quantum-dot materials in which MEG has been reported experimentally include PbS and PbSe[34], PbTe[35], CdSe[36] and Si[37]. In bulk semiconductors, carrier multiplication has been observed for over five decades, including in infrared-bandgap semiconductors such as PbS[38]. There is controversy[32] at present as to the quantitative efficiency and the photon-energy-threshold of carrier multiplication in CQDs and how these compare with bulk semiconductors; but the underlying concept is well accepted, and its prospective value in increasing photovoltaic device efficiency (in the limit, approaching multi-junction performance in a single-junction device) is understood.

An important challenge for making use of MEG is the efficient extraction of the biexcitons and triexcitons that exist within quantum dots. MEG has been reported, based on all-optical spectroscopic data, not only in solution but also in thin solid films. But in spite of numerous attempts within materials systems, and at photon energies, reported to manifest MEG, neither external nor internal quantum efficiency (Table 1) has been shown to exceed 100% (refs 8, 13, 26, 27, 39–41). In particular, one careful and systematic study[42] recently aimed to explore whether a key signature of MEG — an internal quantum efficiency of greater than unity — was observable in the optoelectronic properties of a low-bandgap PbSe CDQ photovoltaic device. Once reflection and absorption were carefully taken into account, internal quantum efficiencies approaching, but not exceeding, 100% were reported.

Two practical obstacles must be overcome to show efficient MEG harvesting in photovoltaic devices. MEG has recently been shown to be sensitive to the chemical nature of the CQD surface; and, as discussed above, so too has photovoltaic device performance. Initial studies[43] indicate that the thiol-based surface treatments, so effective in producing efficient photovoltaic devices, curtail MEG efficiency. Second, carrier extraction of multiple excitons will be considerably more challenging still than when extracting single electron–hole pairs. Whereas single excitons may survive microseconds in PbS CQDs, multiple excitons will recombine through the Auger process within less than 100 ps. In the most optimistic scenario for MEG carrier extraction, in which a significant built-in potential falls

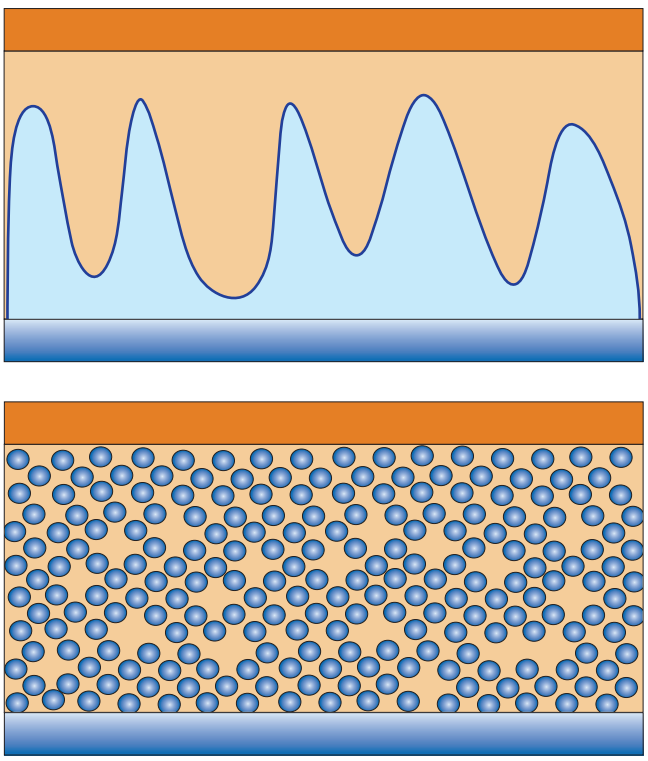


**Figure 6 | Breaking the extraction–absorption compromise through nanostructuring. a**, Analogue of a bulk heterojunction device, in which two phases form a high-surface-area charge-separating junction. **b**, A nanoporous architecture, in which a transparent electrode (blue) is first formed and then infiltrated with light-absorbing material (orange) such as colloidal quantum dots.

across a single layer of dots, carrier extraction within 50 ps requires an effective mobility of greater than $10^{-2}$ cm$^2$ V$^{-1}$ s$^{-1}$, greater than has so far been reported in CQD photovoltaic devices. Efficient multi-exciton harvesting may, like solution-processed photovoltaic devices in general, therefore depend on further strides in improving charge carrier transport in colloidal quantum-dot solids.

## Conclusion

The performance of solution-processed infrared photovoltaics is now within range of doubling the overall solar power conversion of organic photovoltaics by stacking to form a multi-junction cell. The achievement of a all-solid-state solution-processed photovoltaic device with AM1.5 power conversion efficiency of around 10% would offer a new and powerful combination of power conversion efficiency, cost and flexibility. Progress remains to be made on a number of key fronts, drawing on advances in materials chemistry, device fabrication and device modelling, for this ambitious goal to be realized. The rapid rate of progress of the field, combined with the existence of clear further avenues for device optimization, suggests that solution-processed infrared photovoltaics have a promising future.

## References

1. Schurig, D. *et al.* Metamaterial electromagnetic cloak at microwave frequencies. *Science* **314,** 977–980 (2006).
2. *Min*, B. *et al.* High-Q surface-plasmon-polariton whispering-gallery microcavity. *Nature* **457,** 455–458 (2009).
3. Nelson, J. in *Physics of Solar Cells* 450 (World Scientific, 2003).
4. King, R. R. Multijunction cells: Record breakers. *Nature Photon.* **2,** 284–286 (2008).
5. Green, M. A., Emery, K., Hishikawa, Y. & Warta, W. Solar cell efficiency tables (Version 33). *Prog. Photovolt. Res. Applic.* **17,** 85–94 (2009).

6. Shah, A., Torres, P., Tscharner, R., Wyrsch, N. & Keppner, H. Photovoltaic technology: The case for thin-film solar cells. *Science* **285,** 692–698 (1999).
7. Klem, E. J. D., MacNeil, D. D., Cyr, P. W., Levina, L. & Sargent, E. H. Efficient solution-processed infrared photovoltaic cells: Planarized all-inorganic bulk heterojunction devices via inter-quantum-dot bridging during growth from solution. *Appl. Phys. Lett.* **90,** 183113 (2007).
8. Johnston, K. W. *et al.* Schottky-quantum dot photovoltaics for efficient infrared power conversion. *Appl. Phys. Lett.* **92,** 151115 (2008).
9. Koleilat, G. *et al.* Efficient, stable infrared photovoltaics based on solution-cast colloidal quantum dots. *ACS Nano* **2,** 833–840 (2008).
10. Luther, J. M. *et al.* Schottky solar cells based on colloidal nanocrystal films. *Nano Lett.* **8,** 3488 (2008).
11. Klem, E. J. D., MacNeil, D. D., Levina, L. & Sargent, E. H. Solution processed photovoltaic devices with 2% infrared monochromatic power conversion efficiency: Performance optimization and oxide formation. *Adv. Mater.* **20,** 3433–3439 (2008).
12. Winder, C. & Sariciftci, N. S. Low bandgap polymers for photon harvesting in bulk heterojunction solar cells. *J. Mater. Chem.* **14,** 1077–1086 (2004).
13. Johnston, K. W. *et al.* Efficient Schottky-quantum-dot photovoltaics: The roles of depletion, drift, and diffusion. *Appl. Phys. Lett.* **92,** 122111 (2008).
14. Clifford, J. P., Johnston, K. W., Levina, L. & Sargent, E. H. Schottky barriers to colloidal quantum dot films. *Appl. Phys. Lett.* **91,** 253117 (2007).
15. Coakley, K. M. & McGehee, M. D. Conjugated polymer photovoltaic cells. *Chem. Mater.***16,** 4533–4542 (2004).
16. Clifford, J. P. *et al.* Fast, sensitive and spectrally tuneable colloidal-quantum-dot photodetectors. *Nature Nanotech.* **4,** 40–44 (2009).
17. Blom, P. W. M., Mihailetchi, V. D., Koster, L. J. A. & Markov, D. E. Device physics of polymer: Fullerene bulk heterojunction solar cells. *Adv. Mater.* **19,** 1551–1566 (2007).
18. Halls, J. J. M. *et al.* Efficient photodiodes from interpenetrating polymer networks. *Nature* **376,** 498–500 (1995).
19. Yu, G., Gao, J., Hummelen, J. C., Wudl, F. & Heeger, A. J. Polymer photovoltaic cells: Enhanced efficiencies via a network of internal donor–acceptor heterojunctions. *Science* **270,** 1789–1791 (1995).
20. O'Regan, B. & Grätzel, M. A low-cost, high-efficiency solar cell based on dye-sensitized colloidal $TiO_2$ films. *Nature* **353,** 737–740 (1991).
21. Konstantatos, G. *et al.* Ultrasensitive solution-cast quantum dot photodetectors. *Nature* **442,** 180–183 (2006).
22. Hoogland, S. *et al.* Megahertz-frequency large-area optical modulators at 1.55 μm based on solution-cast colloidal quantum dots. *Opt. Express* **16,** 6683–6691 (2008).
23. Dadosh, T. *et al.* Measurement of the conductance of single conjugated molecules. *Nature* **436,** 677–680 (2005).
24. Talapin, D. V. & Murray, C. B. Applied physics: PbSe nanocrystal solids for n- and p-channel thin film field-effect transistors. *Science* **310,** 86–89 (2005).
25. Barkhouse, D. A. R., Pattantyus-Abraham, A. G., Levina, L. & Sargent, E. H. Thiols passivate recombination centers in colloidal quantum dots leading to enhanced photovoltaic device efficiency. *ACS Nano* **2,** 2356–2362 (2008).
26. Koleilat, G. I. *et al.* Efficient, stable infrared photovoltaics based on solution-cast colloidal quantum dots. *ACS Nano* **2,** 833–840 (2008).
27. Luther, J. M. *et al.* Structural, optical, and electrical properties of self-assembled films of PbSe nanocrystals treated with 1,2-ethanedithiol. *ACS Nano* **2,** 271–280 (2008).
28. Westenhoff, S. *et al.* Charge recombination in organic photovoltaic devices with high open-circuit voltages. *J. Am. Chem. Soc.* **130,** 13653–13658 (2008).
29. Konstantatos, G., Levina, L., Fischer, A. & Sargent, E. H. Engineering the temporal response of photoconductive photodetectors via selective introduction of surface trap states. *Nano Lett.* **8,** 1446–1450 (2008).
30. Lee, H. J. *et al.* CdSe quantum dot-sensitized solar cells exceeding efficiency 1% at full-Sun intensity. *J. Phys. Chem. C* **112,** 11600–11608 (2008).
31. Hyun, B. *et al.* Electron injection from colloidal PbS quantum dots into titanium dioxide nanoparticles. *ACS Nano* **2,** 2206–2212 (2008).
32. Nozik, A. J. Multiple exciton generation in semiconductor quantum dots. *Chem. Phys. Lett.* **457,** 3–11 (2008).
33. Klimov, V. I. Detailed-balance power conversion limits of nanocrystal-quantum-dot solar cells in the presence of carrier multiplication. *Appl. Phys. Lett.* **89,** 123118 (2006).
34. Ellingson, R. J. *et al.* Highly efficient multiple exciton generation in colloidal PbSe and PbS quantum dots. *Nano Lett.* **5,** 865–871 (2005).
35. Murphy, J. E. *et al.* PbTe colloidal nanocrystals: Synthesis, characterization, and multiple exciton generation. *J. Am. Chem. Soc.* **128,** 3241–3247 (2006).
36. Schaller, R. D., Sykora, M., Jeong, S. & Klimov, V. I. High-efficiency carrier multiplication and ultrafast charge separation in semiconductor nanocrystals studied via time-resolved photoluminescence. *J. Phys. Chem. B* **110,** 25332–25338 (2006).
37. Beard, M. C. *et al.* Multiple exciton generation in colloidal silicon nanocrystals. *Nano Lett.* **7,** 2506–2512 (2007).
38. Smith, A. & Dutton, D. Behavior of lead sulfide photocells in the ultraviolet. *J. Opt. Soc. Am.* **48,** 1007 (1958).
39. Law, M. *et al.* Structural, optical, and electrical properties of PbSe nanocrystal solids treated thermally or with simple amines. *J. Am. Chem. Soc.* **130,** 5974–5985 (2008).
40. Luque, A., Martí, A. & Nozik, A. J. Solar cells based on quantum dots: Multiple exciton generation and intermediate bands. *MRS Bull.* **32,** 236–241 (2007).
41. Jiang, X. *et al.* PbSe nanocrystal/conducting polymer solar cells with an infrared response to 2 micron. *J. Mater. Res.***22,** 2204–2210 (2007).
42. Law, M. *et al.* Determining the internal quantum efficiency of PbSe nanocrystal solar cells with the aid of an optical model. *Nano Lett.* **8,** 3904 (2008).
43. Beard, M. C. *et al.* Variations in the quantum efficiency of multiple exciton generation for a series of chemically treated PbSe nanocrystal films. *Nano Lett.* **9,** 836–845 (2009).
44. Wang, X. *et al.* Infrared photocurrent spectral response from plastic solar cell with low-band-gap polyfluorene and fullerene derivative. *Appl. Phys. Lett.* **85,** 5081–5083 (2004).
45. Mcdonald, S. A. *et al.* Solution-processed PbS quantum dot infrared photodetectors and photovoltaics. *Nature Mater.* **4,** 138–142 (2005).
46. Wang, X. *et al.* Enhanced photocurrent spectral response in low-bandgap polyfluorene and $C_{70}$-derivative-based solar cells. *Adv. Funct. Mater.* **15,** 1665–1670 (2005).
47. Zhang, S., Cyr, P. W., McDonald, S. A., Konstantatos, G. & Sargent, E. H. Enhanced infrared photovoltaic efficiency in PbS nanocrystal/semiconducting polymer composites: 600-fold increase in maximum power output via control of the ligand barrier. *Appl. Phys. Lett.* **87,** 1–3 (2005).
48. Maria, A., Cyr, P. W., Klem, E. J. D., Levina, L. & Sargent, E. H. Solution-processed infrared photovoltaic devices with >10% monochromatic internal quantum efficiency. *Appl. Phys. Lett.* **87,** 1–3 (2005).
49. Wienk, M. M., Turbiez, M. G. R., Struijk, M. P., Fonrodona, M. & Janssen, R. A. J. Low-band gap poly(di-2-thienylthienopyrazine):fullerene solar cells. *Appl. Phys. Lett.* **88,** 153511 (2006).
50. Gunes, S. *et al.* Hybrid solar cells using PbS nanoparticles. *Solar Energy Mater. Solar Cells* **91,** 420–423 (2007).
51. Sun, M. *et al.* Near-infrared response photovoltaic device based on novel narrow band gap small molecule and PCBM fabricated by solution processing. *Solar Energy Mater. Solar Cells* **91,** 1681–1687 (2007).
52. Dissanayake, D. M. N. M. *et al.* A PbS nanocrystal–$C_{60}$ photovoltaic device for infrared light harvesting. *Appl. Phys. Lett.* **91,** 133506 (2007).
53. Perzon, E. *et al.* A conjugated polymer for near infrared optoelectronic applications. *Adv. Mater.* **19,** 3308–3311 (2007).
54. Henry, C. H. Limiting efficiencies of ideal single and multiple energy gap terrestrial solar cells. *J. Appl. Phys.* **51,** 4494–4500 (1980).


## Acknowledgements

I thank S. Hinds for producing the spatial band diagrams of Fig. 4.